Biochemical and Biophysical Research Communications 500 (2018) 698–703

Contents lists available at ScienceDirect

Biochemical and Biophysical Research Communications

journal homepage: www.elsevier.com/locate/ybbrc

Crystal structure of a thermophilic O^6-alkylguanine-DNA alkyltransferase-derived self-labeling protein-tag in covalent complex with a fluorescent probe

Franca Rossi [a], Castrese Morrone [a], Alberto Massarotti [a], Davide Maria Ferraris [a, c], Anna Valenti [b], Giuseppe Perugino [b, **], Riccardo Miggiano [a, c, *]

[a] DSF-Dipartimento di Scienze del Farmaco, University of Piemonte Orientale, Via Bovio 6, 28100 Novara, Italy
[b] Institute of Biosciences and BioResources, National Research Council of Italy, Via Pietro Castellino 111, 80131 Naples, Italy
[c] IXTAL srl, via Bovio 6, 28100, Novara, Italy

ARTICLE INFO

Article history:
Received 12 April 2018
Accepted 17 April 2018
Available online 30 April 2018

Keywords:
O^6-alkylguanine-DNA alkyltransferase
Self-labeling protein tag
Fluorescent probe
Extremophiles
Crystal structure

ABSTRACT

The self-labeling protein tags are robust and versatile tools for studying different molecular aspects of cell biology. In order to be suitable for a wide spectrum of experimental conditions, it is mandatory that these systems are stable after the fluorescent labeling reaction and do not alter the properties of the fusion partner. *Ss*OGT-H^5 is an engineered variant alkylguanine-DNA-alkyl-transferase (OGT) of the hyperthermophilic archaeon *Sulfolobus solfataricus*, and it represents an alternative solution to the SNAP-tag® technology under harsh reaction conditions.

Here we present the crystal structure of *Ss*OGT-H^5 in complex with the fluorescent probe SNAP-Vista Green® (*Ss*OGT-H^5-SVG) that reveals the conformation adopted by the protein upon the trans-alkylation reaction with the substrate, which is observed covalently bound to the catalytic cysteine residue. Moreover, we identify the amino acids that contribute to both the overall protein stability in the post-reaction state and the coordination of the fluorescent moiety stretching-out from the protein active site. We gained new insights in the conformational changes possibly occurring to the OGT proteins upon reaction with modified guanine base bearing bulky adducts; indeed, our structural analysis reveals an unprecedented conformation of the active site loop that is likely to trigger protein destabilization and consequent degradation. Interestingly, the SVG moiety plays a key role in restoring the interaction between the N- and C-terminal domains of the protein that is lost following the new conformation adopted by the active site loop in the *Ss*OGT-H^5-SVG structure. Molecular dynamics simulations provide further information into the dynamics of *Ss*OGT-H^5-SVG structure, highlighting the role of the fluorescent ligand in keeping the protein stable after the trans-alkylation reaction.

1. Introduction

The fluorescent labeling of proteins is a powerful approach to study any aspects of the biology of the cell, including protein function, localization, trafficking and macromolecular interaction networks, both *in vitro* and *in vivo*. In many cases, the labeling is achieved by expressing a chimera, in which the protein of interest is fused to a polypeptide (*i.e.* tag) that behaves as the traceable moiety for protein imaging [1,2]. The self-labeling protein tags specifically and covalently bind different small-molecule fluorophores, a property that finds a huge number of applications [3–7]. A well-characterized example is the SNAP-tag® (New England Biolabs) [8], an engineered form of the hAGT, responsible for alkylated-DNA direct repair [9,10]. AGTs (EC: 2.1.1.63; alternative names: MGMT or OGT) are small suicidal proteins that perform the stoichiometric transfer of the alkyl group from the O^6 position of an alkylated-

Abbreviations: OGT/AGT, O^6-alkylguanine-DNA alkyltransferase; hAGT, human O^6-alkylguanine-DNA alkyltransferase; BG, benzylguanine; SVG, SNAP-Vista Green™ reagent; HTH, Helix-Turn-Helix.

* Corresponding author. DSF-Dipartimento di Scienze del Farmaco, University of Piemonte Orientale, Via Bovio 6, 28100 Novara, Italy.
** Corresponding author.
E-mail addresses: franca.rossi@uniupo.it (F. Rossi), castrese.morrone@uniupo.it (C. Morrone), alberto.massarotti@uniupo.it (A. Massarotti), davide.ferraris@uniupo.it (D.M. Ferraris), anna.valenti@ibbr.cnr.it (A. Valenti), giuseppe.perugino@ibbr.cnr.it (G. Perugino), riccardo.miggiano@uniupo.it (R. Miggiano).

https://doi.org/10.1016/j.bbrc.2018.04.139
0006-291X/

guanine (or from the O^4 position of an alkylated-thymine) to the catalytic cysteine residue of the protein active site [11]. The single-step trans-alkylation reaction brings the base back to the original state, while leaving the protein permanently inactivated and more prone to destabilization and degradation [12,13]. The SNAP-tag® was obtained through a directed protein evolution approach, by introducing 19 amino acid substitutions in the hAGT sequence and by deleting the 25 residues at the C-terminus of the protein [9,10,14]. This engineered protein reacts with BG derivatives bearing a fluorescent substituting group at their O^6 position, such as the SVG reagent [9]. Compared to the parental hAGT the SNAP-tag® displays an enhanced activity and a remarkably improved stability both *in vitro* and when expressed inside the cell. Conversely, the SNAP-tag® does not possess any significant DNA-binding or alkylated-DNA repairing activity, thus satisfying a mandatory requirement to avoid an improper localization or an altered function of the SNAP-tag-fused protein of interest [10].

The SNAP-tag® is generally used for studying mesophilic species [10], whereas a thermostable OGT-based protein-tag could offer a greater exploitability to characterize organisms which are exposed to harsh growth conditions, and a superior intrinsic robustness in *in vitro* experiments requiring a wide range of temperature, pH, ionic strength and the presence of common denaturing agents [15,16]. To this end, an engineered variant of the *Sulfolobus solfataricus* OGT was previously prepared (hereon indicated as *Ss*OGT-H^5), which is characterized by the presence of a number of amino acid substitutions in the catalytic C-terminal domain of the protein. In detail, 5 mutated residues map at the DNA HTH motif (*i.e.* S100A, R102A, G105K, M106T and K110E), and on residue maps at the C-side of the active site loop (S132E), thus only partially matching the point-mutation profile of the hAGT-derived SNAP-tag® [10,15,16]. Nonetheless, thus mutagenesis approach completely abolished the *Ss*OGT-H^5 variant capability to bind the DNA, while preserved the protein self-labeling efficiency in the presence of the SVG probe [15,16]. The SsOGT-H5 properly works as a self-labeling protein-tag both in the mesophilic organism *E. coli*, as well as in thermophilic species as the bacterium *Thermus thermophilus* and the archaeaon *Sulfolobus islandicus* [16,17].

Although the SNAP-tag® and the *Ss*OGT-H^5 proteins have been extensively characterized, a structural snapshot of the protein architecture upon the trans-alkylation reaction with a synthetic probe was missing. We solved and report here the crystal structure of the *Ss*OGT-H^5 protein in covalent complex with the O^6-substituting group of the SVG reagent (abbreviated as *Ss*OGT-H^5-SVG). Beside representing the first crystal structure of a AGT-derived self-labeling protein-tag in complex with a fluorescent probe, our data provide a structural overview of the amino acids that participate in the coordination of the bulky adduct in the post-reaction state of the protein, including an unprecedented role of residues belonging to the poorly functionally characterized N-terminal domain. Moreover, by performing molecular dynamics simulations on the novel *Ss*OGT-H^5-SVG structure, we gained insights into how the overall stability of the *Ss*OGT-H^5 protein could be affected by the presence of the fluorescent moiety in the protein active site. Overall, our analysis could be used for further improving the selectivity of the corresponding *Ss*OGT-H^5-tag/fluorescent substrate system.

2. Material and methods

2.1. Chemicals

All reagents were obtained from Sigma-Aldrich unless otherwise specified.

2.2. Protein expression and purification

The *Ss*OGT-H^5 variant was expressed in the *E. coli* ABLE-C strain and purified as previously described [15,16].

2.3. Crystallization and data collection

In order to prepare the self-labeled *Ss*OGT-H^5 protein to be used in crystallization experiments, a solution of the commercial SVG reagent (250 μM) was mixed with the *Ss*OGT-H^5 protein solution (10 mg/mL in 20 mM phosphate buffer, pH 7.3 and 150 mM NaCl) at a protein:SVG molar ratio of 1:1, and incubated overnight at 4 °C before crystallization trials. The initial crystallization conditions were identified by means of a robot-assisted (Oryx4; Douglas Instruments) sitting-drop-based spare-matrix strategy, using screen kits from Hampton Research and Qiagen, by the vapor diffusion technique.

The *Ss*OGT-H^5-SVG crystals grew to their maximum dimensions in two months at 4 °C in a drop obtained by mixing equal volumes of a 7 mg/mL labeled-protein solution and 2.0 M ammonium sulfate, in a final droplet volume of 1 μL. Single crystals were cryo-protected in the precipitant solution containing 12% glycerol, mounted in a cryo-loop, and flash frozen in liquid nitrogen at 100 K for subsequent X-ray diffraction analysis. The best crystal diffracted at 2.0 Å of resolution at the ID23-2 synchrotron radiation ($\lambda = 0.87$ Å) (European Synchrotron Radiation Facility [ESRF], Grenoble, France). The diffraction data were indexed with XDS program [18], whose indexing score assigned the crystal to the hexagonal space-group P6322 with the cell dimension a = 63.78 Å, b = 63.78 Å, c = 159.04 Å, containing 1 molecule per asymmetric unit, with a corresponding solvent content of 50% and a Matthews coefficient of 2.46 [19]. Further data analysis was carried out using the CCP4 program suite [20]; in particular, the diffraction intensities were scaled and merged with the programs SCALA and TRUNCATE, respectively.

The structure of the *Ss*OGT-H^5-SVG protein was solved by molecular replacement using the program Phaser of the PHENIX software suite [21,22] and the structure of the wild type *Ss*OGT protein as the search model (Protein Data Bank [PDB] accession number: 4ZYE). The SVG scaffold to be fitted in the correspondent electron density was drawn with ACD/ChemSketch chemical drawing package, whereas the ligand coordinates and restraints were generated using ELBOW of the PHENIX software suite [22]. The resulting electron density map was of good quality, allowing manual model building, using the program Coot [23]. The programs PHENIX and Refmac [20,22] were used for crystallographic refinement and to add water molecules. Data collection and refinement statistics are summarized in Table 1. The atomic coordinates and structure factors of the H^5-SVG have been deposited in the PDB (http://www.rcsb.org/) under the accession number 6GA0.

All figures have been generated using PyMol (https://www.pymol.org).

2.4. Molecular dynamics (MD)

The atomic coordinates of the *Ss*OGT-H^5-SVG protein were used for the initial state of the MD simulations, either including or omitting the SVG molecule coordinates. The MD protocol was performed as previously reported [24]. Two series of simulations were carried out: at a constant temperature of 353 K, since the *Ss*OGT-H^5 is a hyperthermophilic protein, and at a constant temperature of 500 K, to analyze the protein unfolding.

Table 1
Data collection, phasing, and refinement statistics.

	*Ss*OGT-H^5-SVG
Data collection	
Space Group	P6322
Unit cell	a = b = 63.779 Å c = 159.038 Å α = β = 90° λ = 120°
Wavelength (Å)	0.873
Resolution (Å)	2.00
Total reflections	178930 (26432)
Unique reflections	13435 (1296)
Mean(I)/sd(I)	27.8 (5.8)[a]
Completeness (%)	98.3 (99.2)[a]
Multiplicity	13.3 (13.8)[a]
R_{merge} (%)	6.2
R_{meas} (%)	6.5
Refinement	
Rfactor/Rfree (%)	18.0/22.0
Protein Atoms	1220
Ligand atoms	46
Water molecules	95
R.m.s.d. bonds (Å)	0.019
R.m.s.d. angles (°)	2.04
Average B (Å^2)	
Protein	31.0
Ligand	34.2
Solvent	37.6

[a] Values in parentheses refer to the highest resolution shell.

3. Results and discussion

3.1. Structural analysis of the SVG-labeled SsOGT-H^5 variant

SVG-labeled *Ss*OGT-H^5 produced crystals of remarkable quality that diffracted at 2.0 Å resolution, indicative of the structural integrity of the ligand-protein covalent adduct. Notably, the high-quality electron density map allowed us to model the SVG-Cys119 covalent adduct resulting from the trans-alkylation reaction, and to unambiguously assign the conformation adopted by the carboxyfluorescein diacetate N-succinimidyl ester moiety of the ligand to the para-isomer (Fig. 1, inset). As described for all of the AGT proteins [11,24–30] the *Ss*OGT-H^5-SVG protein architecture (Fig. 1) consists of two roughly globular domains connected by a long loop that display the same overall fold observed in the crystal structures of the parental *Ss*OGT protein in its ligand-free, DNA-bound or methylated form [26].

The N-terminal domain of *Ss*OGT-H^5-SVG is built up by a three-stranded β-sheet connected to a conserved α-helix (h1) by a random-coiled region (residues 28–39). The peculiar Cys29-Cys31 disulfide bridge, which is observable in all of the *Ss*OGT structures, is not affected by the presence of the fluorophore tri-cyclic moiety that protrudes out the catalytic cavity. Instead, by acting as a rigid constraint at the N-side of the random coil, the disulfide bridge appears to assist the orientation of the bulky SVG group towards the boundary region between the active site loop and the α-helix 5 (h5) of the C-terminal domain on one side, and the short loop connecting the β1 and β2 strands of the N-terminal domain on the opposite one (Fig. 1). As illustrated in Fig. 2, the interaction of the SVG ligand with the N-terminal domain is based on direct or water-mediated hydrogen bonds, which are contributed by the Gly12 and Tyr13 backbone nitrogen atoms, or by the Asp27 carboxylic group.

Further, the SVG adduct is stabilized by the C-terminal moiety of the symmetry mate, which provides a network of hydrogen bonds involving the carboxylic group of Glu110, the hydroxyl group of Tyr131 and the guanidine group of Arg133 which lock the tri-cyclic xanthen-moiety portion of SVG. (Supplemental Fig. S1).

As mentioned above, the 6 amino acid substitutions that characterize the *Ss*OGT-H^5 variant are placed at the C-terminal domain of the protein, which houses all the functional elements required to sustain the catalysis: the HTH motif, which encompass the recognition α-helix h4 that plays a crucial role in properly positioning the alkylated-base inside the active site upon DNA binding; the “Asn hinge” which connects the h4 to the highly conserved PCHRV catalytic signature; the active site loop and the α-helix h5 that together build up the ligand binding cavity wall opposing the one constituted by the HTH and the “Asn hinge” (Fig. 1). Besides the covalent bond of the catalytic Cys119 with SVG (see above), the h5 residue Leu137 is observed in hydrophobic contact with the benzyl ring linked to the SVG tri-cyclic xanthen-moiety (at a distance of ~3.8 Å), while the Cδ and Cε atoms of Leu114 are involved in a weak interaction to the SVG benzyl ring covalently bound to the Cys119 (at a mean 4.5 Å distance of) (Fig. 2). Previous biochemical and structural analysis revealed that two point mutations in the recognition helix are mainly responsible for the loss of DNA-binding activity observed for the SNAP-tag® when compared to wild-type hAGT: R128A and G131K [10,14]. For this reason, the same amino acid substitutions were introduced in the *Ss*OGT-H^5 variant (i.e. R102A and G105K, respectively) [15,16]. Similar to what has been observed in the crystal structure of the SNAP-tag® [10], in the *Ss*OGT-H^5-SVG structure, the side chain of the Lys105 residue is oriented towards the active site loop, on the opposing side of the active site (Fig. 1), overall narrowing the ligand binding cavity entrance. Such conformation could participate to the suppression of the DNA-binding activity of *Ss*OGT-H^5, which was observed in EMSA experiments [15]. Indeed, the side chain of Lys105 would collide with the sugar-phosphate backbone of the DNA substrate, and consequently would hamper a proper housing of the modified base inside the active site. Notably, this effect could be exacerbated by the concomitant mutation of the strictly conserved Arg102 that replaces the flipped-out modified base in the regular DNA base stacking.

3.2. The active site loop of the SsOGT-H^5-SVG undergoes a conformational rearrangement

A comparison of the crystal structures of *Ss*OGT-H^5-SVG and both the ligand-free *Ss*OGT (PDB: 4ZYE) and methylated *Ss*OGT (PDB: 4ZYG) [26] highlights a relevant difference at the level of the conformation of the active site loop (aa. 125–134), that appears much more exposed to the solvent, as a possible consequence of the steric hindrance of the SVG adduct at the interface between the N- and the C-terminal domain of the *Ss*OGT-H^5 protein (Fig. 3A). Considering the slightly higher sensitivity of *Ss*OGT-H^5-SVG to proteolytic cleavage compared to that of the unreacted *Ss*OGT-H^5 [16], we speculate that the active site loop rearrangement, which could follow the self-labeling reaction, turns the protein in a state more prone to proteolytic attack [31]. Moreover, the active site loop conformation observed in the *Ss*OGT-H^5-SVG structure, provides structural proof of the proposed rationale by which the flexibility of this region could play a role in modulating the OGTs active site accessibility and overall its structural plasticity, that could favor the hosting of bulky adducts [32].

It was demonstrated that in hAGT the trans-alkylation reaction is accompanied by the loss of a hydrogen bond network that is coordinated by the side chain of the active site cysteine, and induces a steric hindrance-driven displacement of the HTH recognition helix [33]. In the *Ss*OGT structure, the methylation of Cys119 is also accompanied by the repositioning of the Arg133 side chain, that leads to a 1.9 Å movement of the active site loop toward the solvent [24,26]. This phenomenon is exacerbated in the *Ss*OGT-H^5-SVG structure, where the presence of SVG interferes with the inter-domain ionic lock based on the Asp27-Arg133 interaction, and

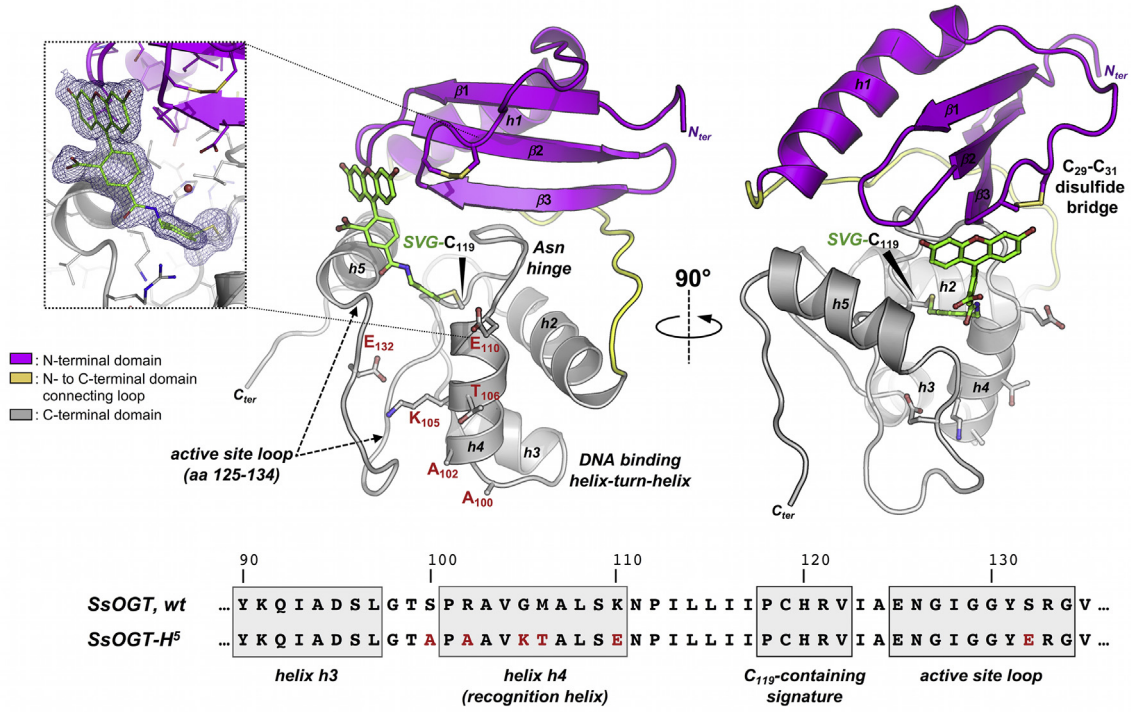

Fig. 1. Crystal structure of *Ss*OGT-H^5-SVG. Cartoon representation of the *Ss*OGT-H^5-SVG structure, as observed from two points of view. In both images, the N-terminal domain, the C-terminal domain, and the connecting loop are colored in magenta, yellow, and grey, respectively. The catalytic cysteine residue (Cys119) covalently bound to SVG fluorescent moiety (green) is drawn as ball-and-stick. Functional elements labeling and secondary structure elements numbering appear in the image together with the mutagenized residues of *Ss*OGT-H^5. Inset: close up view of the SVG group with the corresponding σ_A-weighted 2Fo-Fc electron density (contoured at 1.0 σ). The lower panel shows the sequence alignment of the C-terminal domain region 90–136 of the *Ss*OGT *wild type* and *Ss*OGT-H^5 variant; the mutated residues are highlighted in red.

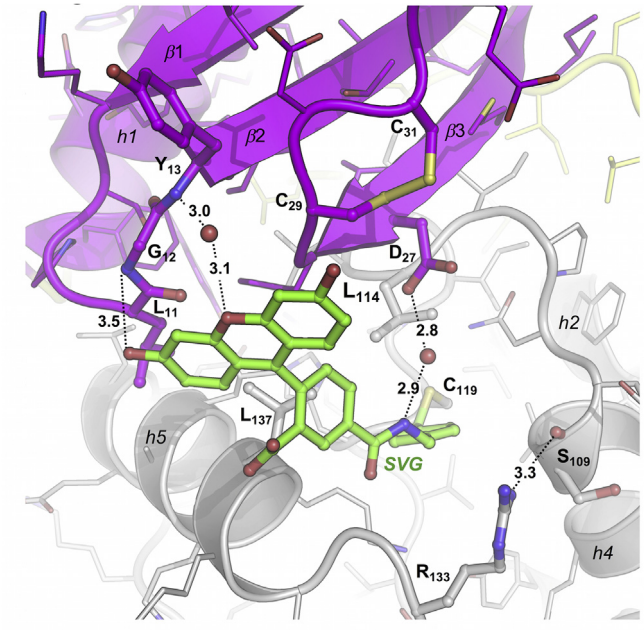

Fig. 2. - The SVG moiety is stabilized by protein residues belonging to both N- and C-terminal domains - Close-up view of the bonding network established by SVG with the indicated protein residues. The SVG moiety and the key amino acids mentioned throughout the text are rendered as ball-and-stick.

induces a relevant displacement of Arg133, at 7.4 Å distance from the N-terminal domain (Fig. 3A). The overall conformation adopted by the *Ss*OGT-H^5-SVG active site loop coordinates the building up of a hydrogen bond network between the opposing walls of the protein active site (Fig. 3B). In particular, the NH_2-group of the recognition helix Lys105 residue (which replaces the wild-type glycine), is observed at a 3.0 Å distance from the carbonylic oxygen atoms of Gly129 and Tyr131, whereas the Lys105 side chain is in hydrophobic contact with the side chain of the Ile128 belonging to the active site loop. Furthermore, the Glu132 residue (which replaces the wild-type serine) establishes a bipartite contact to the Lys138 residue of h5 and the Tyr90 residue of the α-helix 3 (h3) of the HTH motif on the opposite side. The resulting network of extended molecular contacts could mitigate the intrinsic flexibility of the *Ss*OGT-H^5-SVG active site loop in its solvent-exposed conformation.

Moreover, although the SVG ligand disrupts the Asp27-Arg133 interaction at the interface between the N- and C-terminal domains of the protein, it establishes contacts with residues mapping at both domains, restoring the inter-domain communication which likely contributes to protein stability [24,26].

3.3. Molecular dynamics (MD) simulations

In order to obtain independent information on the possible role of the *Ss*OGT-H^5 residues in the SVG moiety coordination, and therefore in protein stability upon the self-labeling reaction, we followed the mobility of the protein residues by MD simulations, using a previously reported protocol [24]. The MD of *Ss*OGT-H^5-SVG was simulated for 100 ns at 500 K (227 °C) to interpret the effect of SVG on structural changes. In order to obtain further insights into the dynamics of the structure, the PCA was used to dissect out cooperative inner motions. In the *Ss*OGT-H^5-SVG (Fig. 4) at 500 K, the internal molecular motion shows a higher stability in both the C-terminal and N-terminal domains of the protein. The

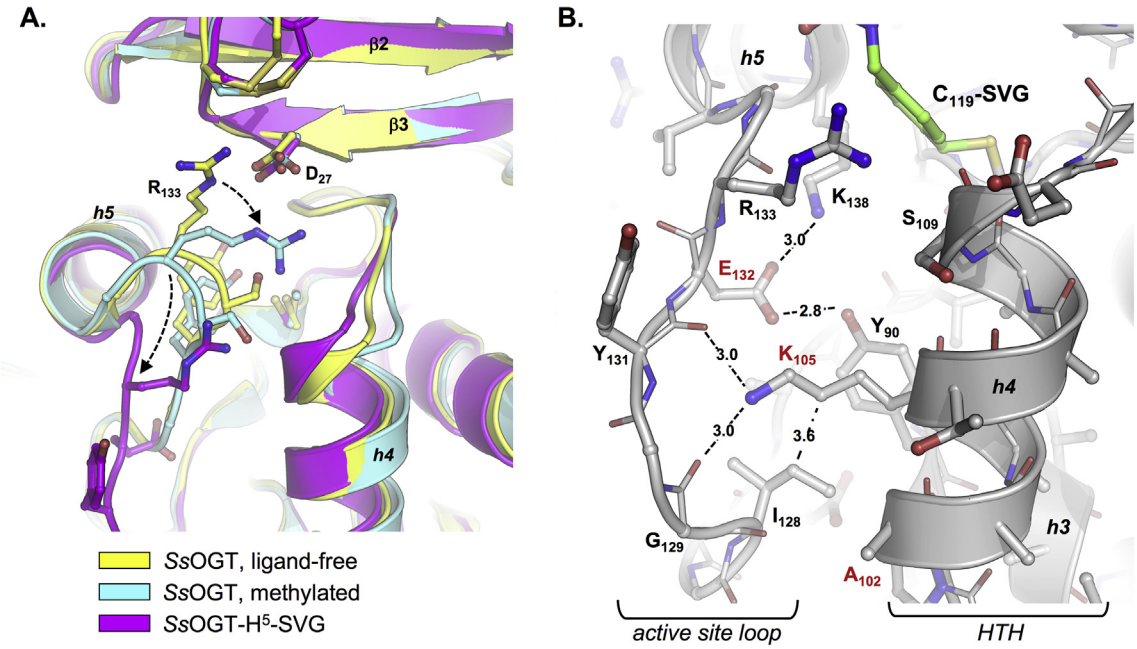

Fig. 3. - Comparison of the crystal structures of *Ss*OGT-H^5-SVG with wild type *Ss*OGT or its methylated form - (A) Cartoon representation of optimally superimposed *Ss*OGT-H^5-SVG structure (magenta) with those of un-reacted *Ss*OGT (yellow) (PDB: 4ZYE; average rmsd = 0.55 Å) and of methylated *Ss*OGT (cyan) (PDB: 4ZYG; average rmsd = 0.57 Å). As a matter of clarity, the SVG moiety has been removed. (B) Close-up of the active site loop conformation as observed in the *Ss*OGT-H^5-SVG structure; the protein residues involved in hydrogen bond network are rendered as ball-and-stick.

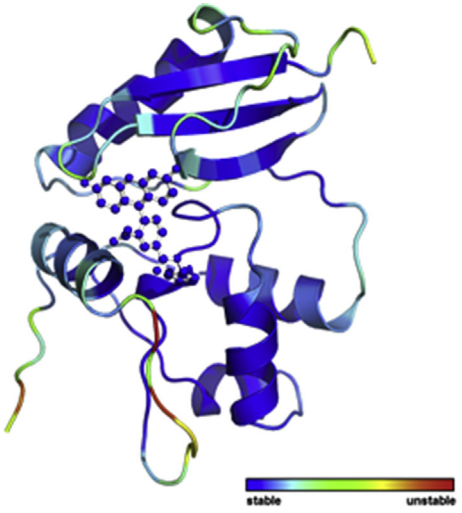

Fig. 4. - PCA analysis of *Ss*OGT-H^5-SVG MD simulations. PCA analysis was performed to analyze the dynamics of residues during the MD simulations performed at 500 K. A color scale is used to indicate the stable (blue) and unstable (red) portions of the protein structures.

only significant movements of residues, affecting both their backbone and side chains atoms, are located in the active site loop. The analysis suggests that the stability of the *Ss*OGT-H^5-SVG structure depends on covalent bonding between SVG and the protein. The effect of SVG on protein stability is more evident if we consider the MD simulation on H^5-SVG in which the SVG moiety has been manually omitted. As expected, the protein structure is less stable, as signaled by the increase of the overall molecular internal motion (Fig. S2).

Taken as a whole our analyses should direct future experiments aimed at enhancing the stability of the AGT-derived protein tags. Indeed, besides the already performed optimization of the protein C-terminal domain (*i.e* to avoid DNA-binding and improve catalysis), further site-directed mutagenesis experiments should target also selected N-terminal residues, by introducing amino acids with the potential capability to interact with the solvent-exposed moiety of the fluorescent probes, finally increasing the *in vitro* stability of the labeled protein and consequently its half-life in the cellular context.

Funding

This work was supported by Fondazione Cariplo (Ricerca biomedica condotta da giovani ricercatori, project 2016-0604).

Acknowledgments

The authors acknowledge the European Synchrotron Radiation Facility (Grenoble, France) for provision of synchrotron radiation at beam line ID23-2. We gratefully acknowledge the support of NVIDIA Corporation with the donation of the Titan X Pascal GPU used for this research.

Appendix A. Supplementary data

Supplementary data related to this article can be found at https://doi.org/10.1016/j.bbrc.2018.04.139.

Transparency document

Transparency document related to this article can be found online at https://doi.org/10.1016/j.bbrc.2018.04.139.

References

[1] B.N.G. Giepmans, S.R. Adams, M.H. Ellisman, R.Y. Tsien, The fluorescent toolbox for assessing protein location and function, Science 312 (2006) 217–224.
[2] M.J. Hinner, K. Johnsson, How to obtain labeled proteins and what to do with

them, Curr. Opin. Biotechnol. 21 (2010) 766–776.
[3] A.A. Hoskins, L.J. Friedman, S.S. Gallagher, D.J. Crawford, E.G. Anderson, R. Wombacher, N. Ramirez, V. W.Cornish, J. Gelles, M.J. Moore, Ordered and dynamic assembly of single spliceosomes, Science 331 (2011) 1289–1295.
[4] T. Klein, A. Löschberger, S. Proppert, S. Wolter, S. van de Lindeand, M. Sauer, Live-cell dSTORM with SNAP-tag fusion proteins, Br. J. Pharmacol. 8 (2011) 7–9.
[5] A. Gautier, E. Nakata, G. Lukinavicius, K.T. Tan, K. Johnsson, Selective cross-linking of interacting proteins using self-labeling tags, J. Am. Chem. Soc. 131 (2009) 17954–17962.
[6] C. Chidley, H. Haruki, M.G. Pedersen, E. Muller, K. Johnsson, A yeast-based screen reveals that sulfasalazine inhibits tetrahydrobiopterin biosynthesis, Nat. Chem. Biol. 7 (2011) 375–383.
[7] K. Bojkowska, F. Santoni de Sio, I. Barde, S. Offner, S. Verp, C. Heinis, K. Johnsson, D. Trono, Measuring in vivo protein half-life, Chem. Biol. 18 (2011) 805–815.
[8] S. Gendreizig, M. Kindermann, K. Johnsson, Induced protein dimerization in vivo through covalent labeling, J. Am. Chem. Soc. 125 (2003) 14970–14971.
[9] A. Keppler, S. Gendreizig, T. Gronemeyer, H. Pick, H. Vogel, K. Johnsson, A general method for the covalent labeling of fusion proteins with small molecules in vivo, Nat. Biotechnol. 21 (2003) 86–89.
[10] B. Mollwitz, E. Brunk, S. Schmitt, F. Pojer, M. Bannwarth, M. Schiltz, U. Rothlisberger, K. Johnsson, Directed evolution of the suicide protein O6-alkylguanine-DNA alkyltransferase for increased reactivity results in an alkylated protein with exceptional stability, Biochemistry 51 (2012) 986–994.
[11] A.E. Pegg, Multifaceted roles of alkyltransferase and related proteins in DNA repair, DNA damage, resistance to chemotherapy, and research tools, Chem. Res. Toxicol. 24 (2011) 618–639.
[12] S. Kanugula, K. Goodtzova, A.E. Pegg, Probing of conformational changes in human O6-alkylguanine-DNA alkyl transferase protein in its alkylated and DNA-bound states by limited proteolysis, Biochem. J. 329 (1998) 545–550.
[13] M. Xu-Welliver, A.E. Pegg, Degradation of the alkylated form of the DNA repair protein, O(6)-alkylguanine-DNA alkyltransferase, Carcinogenesis 23 (2002) 823–830.
[14] A. Juillerat, T. Gronemeyer, A. Keppler, S. Gendreizig, H. Pick, H. Vogel, K. Johnsson, Directed evolution of O6-alkylguanine-DNA alkyltransferase for efficient labeling of fusion proteins with small molecules in vivo, Chem. Biol. 10 (2003) 313–317.
[15] G. Perugino, A. Vettone, G. Illiano, A. Valenti, M.C. Ferrara, M. Rossi, M. Ciaramella, Activity and regulation of archaeal DNA alkyltransferase: conserved protein involved in repair of DNA alkylation damage, J. Biol. Chem. 287 (2012) 4222–4231.
[16] A. Vettone, M. Serpe, A. Hidalgo, J. Berenguer, G. del Monaco, A. Valenti, M. Ciaramella, G. Perugino, A novel thermostable protein-tag: optimization of the Sulfolobus solfataricus DNA-alkyl-transferase by protein engineering, Extremophiles 20 (2016) 1–13.
[17] V. Visone, W. Han, G. Perugino, G. Del Monaco, Q. She, M. Rossi, A. Valenti, M. Ciaramella, In vivo and in vitro protein imaging in thermophilic archaea by exploiting a novel protein tag, PLoS One 10 (2017), e0185791.
[18] W. Kabsch, XDS, Acta Crystallogr. D 66 (2010) 125–132.
[19] Matthews, J. Mol. Biol. 33 (1968) 491–497.
[20] M.D. Winn, C.C. Ballard, K.D. Cowtan, E.J. Dodson, P. Emsley, P.R. Evans, R.M. Keegan, E.B. Krissinel, A.G. Leslie, A. McCoy, et al., Overview of the CCP4 suite and current developments, Acta Crystallogr. D 67 (2011) 235–242.
[21] A.J. McCoy, R.W. Grosse-Kunstleve, P.D. Adams, M.D. Winn, L.C. Storoni, R.J. Read, Phaser crystallographic software, J. Appl. Crystallogr. 40 (2007) 658–674.
[22] P.D. Adams, P.V. Afonine, G. Bunkóczi, V.B. Chen, I.W. Davis, N. Echols, J.J. Headd, L.W. Hung, G.J. Kapral, R.W. Grosse-Kunstleve, et al., PHENIX: a comprehensive Python-based system for macromolecular structure solution, Acta Crystallogr. D 66 (2010) 213–221.
[23] P. Emsley, K. Cowtan, Coot: model-building tools for molecular graphics, Acta Crystallogr. D Biol. Crystallogr 60 (2004) 2126–2132.
[24] C. Morrone, R. Miggiano, M. Serpe, A. Massarotti, A. Valenti, G. Del Monaco, M. Rossi, F. Rossi, M. Rizzi, G. Perugino, Interdomain interactions rearrangements control the reaction steps of a thermostable DNA alkyltransferase, Biochim. Biophys. Acta 1861 (2017) 86–96.
[25] R. Miggiano, V. Casazza, S. Garavaglia, M. Ciaramella, G. Perugino, M. Rizzi, F. Rossi, Biochemical and structural studies of the Mycobacterium tuberculosis O6-methylguanine methyltransferase and mutated variants, J. Bacteriol. 195 (2013) 2728–2736.
[26] G. Perugino, R. Miggiano, M. Serpe, A. Vettone, A. Valenti, S. Lahiri, F. Rossi, M. Rossi, M. Rizzi, M. Ciaramella, Structure-function relationships governing activity and stability of a DNA alkylation damage repair thermostable protein, Nucleic Acids Res. 43 (2015) 8801–8816.
[27] R. Miggiano, G. Perugino, M. Ciaramella, M. Serpe, D. Rejman, O. Páv, R. Pohl, S. Garavaglia, S. Lahiri, M. Rizzi, Crystal structure of Mycobacterium tuberculosis O6-methylguanine-DNA methyltransferase protein clusters assembled on to damaged DNA, Biochem. J. 473 (2016) 123–133.
[28] H. Hashimoto, T. Inoue, M. Nishioka, S. Fujiwara, M. Takagi, T. Imanaka, Y. Kai, Hyperthermostable protein structure maintained by intra and inter-helix ion-pairs in archaeal O6-methylguanine-DNA methyltransferase, J. Mol. Biol. 292 (1999) 707–716.
[29] A. Roberts, J.G. Pelton, D.E. Wemmer, Structural studies of MJ1529, an O6-methylguanine-DNA methyltransferase, Magn. Reson. Chem. 44 (2006) S71–S82.
[30] M.H. Moore, J.M. Gulbis, E.J. Dodson, B. Demple, P.C. Moody, Crystal structure of a suicidal DNA repair protein: the Ada O6-methylguanineDNA methyltransferase from *E. coli*, EMBO J. 13 (1994) 1495–1501.
[31] C. Park, S. Marqusee, Probing the high energy states in proteins by proteolysis, J. Mol. Biol. 343 (2004) 1467–1476.
[32] R. Miggiano, A. Valenti, F. Rossi, M. Rizzi, G. Perugino, M. Ciaramella, Every OGT is illuminated… by fluorescent and synchrotron lights, Int. J. Mol. Sci. 18 (2017) 2613.
[33] D.S. Daniels, C.D. Mol, A.S. Arval, S. Kanugula, A.E. Pegg, J.A. Tainer, Active and alkylated human AGT structures: a novel zinc site, inhibitor and extrahelical binding. DNA damage reversal revealed by mutants and structures of active and alkylated human AGT, EMBO J. 19 (2000) 1719–1730.